Sigma J Eng & Nat Sci 9 (2), 2018, 175-192

Publications Prepared for the 20. National Mechanics Congress

**Research Article**

# SUPPRESSING THE IRREGULAR FREQUENCIES IN WAVE-BODY INTERACTION PROBLEMS: EFFECT OF DISCRETIZATION ON THE PERFORMANCE OF EXTENDED BOUNDARY INTEGRAL EQUATION METHOD

**Enes TUNCA[1], Aytekin DURANAY[2], Bahadır UĞURLU*[3]**

[1]*Faculty of Naval Architecture and Ocean Engineering, Istanbul Technical University, Maslak-ISTANBUL;* ORCID:0000-0001-9671-4937
[2]*Faculty of Naval Architecture and Ocean Engineering, Istanbul Technical University, Maslak-ISTANBUL;* ORCID:0000-0002-9551-3508
[3]*Faculty of Naval Architecture and Ocean Engineering, Istanbul Technical University, Maslak-ISTANBUL;* ORCID:0000-0001-7923-6777

**Received: 01.02.2018 Accepted: 01.08.2018**

**ABSTRACT**

Within a hydroelastic perspective and through a higher-order implementation, the performance of extended boundary integral equation method (EBIEM) for the removal of irregular frequencies that are inherent to the wave Green function based boundary element solution of the frequency domain wave-body interaction problems is investigated. The fundamental idea of the EBIEM is extending the computational domain by the assumed internal free surface, which is covered by a rigid lid to suppress the non-physical internal fluid motion. The EBIEM is expected to suppress the irregular frequencies completely, though higher-order applications often require a problem dependent analysis for an elimination through a wide frequency range. By focusing on the mesh fineness and element order and selecting two different surface piercing structures–a cylinder and a large floating plate–some general conclusions are drawn.
**Keywords:** Hydroelasticity, extended boundary element method, irregular frequency.

## 1. INTRODUCTION

Hydroelastic analysis of floating structures involves computation of the fluid loads imposed by the surrounding sea environment. Provided that the potential flow model is adopted for describing the fluid motion, the fluid actions can be related with two fundamental components: the radiation potential that describes the perturbations in the fluid domain prescribed by the structural motions and the diffraction component representing the incident and then scattered waves due to the presence of the structure. If the related boundary value problems–i.e., the radiation and diffraction problems–are transformed to boundary integral equations defined over the fluid-structure interface by using the wave Green function and discretely solved by the boundary element method (BEM), then the numerical solution crashes at specific frequencies,

* Corresponding Author: e-mail: bugurlu@itu.edu.tr, tel: (212) 285 64 70

which correspond to the eigenvalues of the non-physical Dirichlet type problem of internal fluid motion, as first pointed by John [1]. This 'irregular frequency' effect results from the fact that the wave Green function satisfies the free surface boundary condition over the whole theoretical free surface–inside and outside of the floating body–even if there is no real fluid inside. The numerical consequence is that the coefficient matrix of the resulting linear system becomes ill-conditioned near each irregular frequency, consequently generating rather erroneous potential distributions within the associated frequency bandwidth. The bandwidths can be reduced, but not eliminated, by using finer meshes, but considering that the irregular frequencies get closer with increasing frequency and their geometry dependent locations cannot be predicted, the practical advantage is limited compared to the computational cost.

Two main approaches that are applied for suppressing the irregular frequencies in wave-body interaction problems are modifying either the integral formulation or the integral domain. Considering that the BEM solution of acoustic radiation problem suffers from the same non-uniqueness problem at certain frequencies, it is not surprising that some of the ideas of acoustics (e.g., Burton and Miller method [2], CHIEF method [3]) are transformed to the field. Kleinman [4] and Lee and Sclavounos [5] combined the fundamental boundary integral equation (BIE) with its normal derivative with respect to the field point (normal BIE). Both BIEs can independently solve the radiation and diffraction problems; the irregular frequencies, however, coincide with the eigenvalues of the interior problem of Dirichlet type for the fundamental BIE and of Neumann type for the normal BIE. By coupling the equations with a complex constant, it is found that the irregular frequencies can be completely removed, meaning that no solution exists for the mixed boundary condition if the same constant is used for proportion. The downside of the technique is that the normal BIE introduces computationally involved hypersingular boundary integrals, which also increases the condition number of the discretized system compared to the main BIE along the entire frequency range, except the irregular frequency regions. Lau and Hearn [6] imposed the constraint that the potential has zero values at certain internal free surface points to achieve a unique solution. Special care must be taken, however, when selecting the interior points; they should not coincide with the nodes of the eigenmodes associated with internal fluid motion. Liapis [7] supplemented the original boundary integral equation with a set of moment-like equations known as the null-field equations. The result is an overdetermined system, which is solved by a least square technique. The extra computational effort is shown to be limited, especially for high frequency range and for bodies having one or two symmetry planes. Considering that the irregular frequencies are associated with the sloshing of the imaginary internal flow, the artificial response can be suppressed by placing a rigid cover over the internal free surface. Ohmatsu [8] demonstrated the idea for the two-dimensional case, and Lee et al [9] proposed an extended boundary integral equation method (EBIEM) as a general low order removal technique by including the internal free surface into the computation domain and applying the rigid wall boundary condition over it. The method may suffer from the increased number of degrees of freedom due to the additional boundary surface and also the condition number generally become an order of magnitude larger compared to the unmodified integral equation. Some of the computational aspects of the EBIEM is lately studied by Liu and Falzarano [10].

The objective of the present study is investigating the performance of the EBIEM for the removal of irregular frequencies within a hydroelastic perspective and through a higher-order BEM implementation. The choice of EBIEM here is mostly related with its straightforward integration to the classical BEM solution of the wave-body interaction problem. The EBIEM is expected to suppress the irregular frequencies completely, though higher-order applications often require a problem dependent analysis for an elimination through a wide frequency range. Reaching out to higher frequencies for analysis, where the disruptive effect of irregular frequencies on solution becomes more severe, might be seen unimportant for routine seakeeping computations that involves the interaction of waves and rigid body motions, but as the flexibility of the structure

increases, the insignificant may become inevitable. Moreover, time domain analysis of ship motions frequently relies on the use of relevant data obtained from the frequency domain analysis instead of the direct solution of the BIE in the time domain; the components of impulse response function and time domain excitation forces are related to their frequency dependent counterparts through the Fourier transform that the accuracy of the frequency domain results over the relevant frequency interval becomes critical. In the study, the focus will be on the effect of internal free surface discretization, in terms of mesh fineness and element order, on regularization of the radiation and wave excitation forces–the major indicators of pollution about irregular frequencies–especially at higher frequencies. Two free surface piercing structures are selected for the analysis: the cylinder serves mostly as a benchmark, to compare the predictions and to demonstrate the effectiveness of the EBIEM for a standard application; the large floating plate, which displays strong influence within a wide frequency band, is the actual case for testing the capacity of the method for hydroelastic behavior.

## 2. FREQUENCY DOMAIN HYDROELASTIC ANALYSIS

### 2.1. Dynamic response of the floating structure

The equation of motion of a floating structure can be given in the discretized form as,

$$\mathbf{M}\ddot{\mathbf{q}}(t) + \mathbf{C}\dot{\mathbf{q}}(t) + \mathbf{K}\mathbf{q}(t) = \mathbf{f}(t) \tag{1}$$

Here, **M**, **C**, and **K** represent the mass, structural damping and stiffness matrices, respectively, **q** stands for the generalized displacements, which includes both the translational and rotational degrees of freedom, **f** is the vector of external forces, and *t* denotes time.
The undamped free vibration of the structure is defined as the response in the absence of damping and external effects, and can be described by substituting the solution $\mathbf{q} = \mathbf{u}e^{i\omega_n t}$ in Eq. (1):

$$(-\omega_n^2\mathbf{M} + \mathbf{K})\mathbf{u} = 0 \tag{2}$$

Solution of the eigenvalue problem (2) gives the dynamic characteristics, i.e., natural frequencies, $\omega_n$, and corresponding normal modes, **u**, of the structure.

The dynamic response of the floating structure can be given as the combination of responses in its normal modes:

$$\mathbf{q}(t) = \sum_{i=1}^{n_m} \mathbf{u}_i p_i(t) = \mathbf{U}\mathbf{p}(t) \tag{3}$$

Here, the modal matrix $\mathbf{U} = \left[\mathbf{u}_1 ..... \mathbf{u}_{n_m}\right]$ describes the $n_m$-dimensional modal space that consists of the considered normal modes, and **p**(*t*) is the principle coordinate vector as the coordinates of the response in the modal space, also representing the participation of individual modes in the overall response; $n_m$ indicates the total number of modes taken into account in the series expansion. The modal matrix includes both the rigid body modes and elastic modes, in general.

By using definition (3) in Eq. (1) and pre-multiplying by $\mathbf{U}^T$, the generalized equation of motion of the floating structure is obtained as,

$$\tilde{\mathbf{M}}\ddot{\mathbf{p}}(t) + \tilde{\mathbf{C}}\dot{\mathbf{p}}(t) + \tilde{\mathbf{K}}\mathbf{p}(t) = \tilde{\mathbf{f}}(t) \tag{4}$$

Here, $\tilde{\mathbf{M}} = \mathbf{U}^{\mathrm{T}}\mathbf{M}\mathbf{U}$, $\tilde{\mathbf{C}} = \mathbf{U}^{\mathrm{T}}\mathbf{C}\mathbf{U}$, $\tilde{\mathbf{K}} = \mathbf{U}^{\mathrm{T}}\mathbf{K}\mathbf{U}$ are the generalized matrices of mass, damping, and stifness, respectively, and $\tilde{\mathbf{f}} = \mathbf{U}^{\mathrm{T}}\mathbf{f}$ is the generalized external force, involving the forces of fluid-structure interaction and wave excitation, and all other external effects.

### 2.2. Wave-structure interaction problem

The viscosity of the fluid gains importance in the thin boundary layer around the floating body and at regions where the flow is considerably separated. Thus, the fluid surrounding the structure can be assumed ideal, i.e. inviscid and incompressible, and its motion is irrotational, so that the fluid velocity vector, **v**, can be taken as the gradient of a velocity potential function $\Phi$ as $\mathbf{v}(\mathbf{x},t)=\nabla\Phi(\mathbf{x},t)$, where $\mathbf{x}=(x, y, z)^{\mathrm{T}}$ denotes the position vector. From the continuity condition, $\Phi$ satisfies the Laplace equation, $\nabla^2\Phi=0$, throughout the fluid domain. Within a linear framework, which requires the fluid reactions are of the first order, the total potential function $\Phi$ can be decomposed into wave diffraction and radiation components that are related with the incoming free surface waves and fluid-structure interaction, respectively:

$$\Phi(\mathbf{x},t)=\Phi_D(\mathbf{x},t)+\Phi_R(\mathbf{x},t) \tag{5}$$

The radiation potential, $\Phi_R$, represents the effects due to the oscillating body in the absence of incident waves; the diffraction potential, $\Phi_D$, represents the incident wave system and its modification because of the floating body, which is assumed in a fixed position. $\Phi_D$ can be further decomposed as $\Phi_D=\Phi_I+\Phi_S$, with $\Phi_I$ and $\Phi_S$ indicating the incident wave potential and scattering wave potential that represents the disturbed wave field due to the presence of the body. $\Phi_I$ for unit amplitude of regular oblique wave propagating in deep water can be given by

$$\Phi_I(\mathbf{x},t)=\frac{ig}{\omega}e^{kz}e^{-i[k(x\cos\alpha+y\sin\alpha)-\omega t]}. \tag{6}$$

Here, $\omega$ and $k$ are the wave frequency and wave number, respectively, $\alpha$ is the incident angle with respect to $x$-axis, and $g$ is the gravitational acceleration. $\omega$ and $k$ are related with the dispersion relation, $k=\omega^2/g$, due to the free surface boundary condition $\partial\Phi_I/\partial z=\left(\omega^2/g\right)\Phi_I$ imposed on the fluid free surface, $S_f$:

A modal expansion similar to Eq. (3), that is used for the structural response, can be adopted for the radiation potential, by proposing a series of potential components corresponding to each considered normal mode:

$$\Phi_R(\mathbf{x},t)=\sum_{i=1}^{n_m}\Phi_i(\mathbf{x})\,p_i(t) \tag{7}$$

Here, $\Phi_i$ is the radiation potential associated with the $i$th normal mode; if the body is enforced to oscillate in the $i$th mode, rigid or elastic, with unit amplitude in otherwise calm water, then the resulting fluid motion will be represented by $\Phi_i$.

The kinematic boundary condition for the velocity potential states the equality of the fluid and body normal velocities over the fluid-body interface, i.e., the wetted surface of the floating structure, $S_w$. Considering Eqs. (3) and (7), for the harmonic motion of the structure experiencing regular waves of frequency $\omega$, the kinematic boundary condition can be given for the radiation potential by

$$\partial\Phi_i/\partial n=i\omega n_i \quad (i=1-3) \tag{8}$$

$$\partial\Phi_i/\partial n=i\omega\left(\mathbf{r}\times\mathbf{n}\right)_{i-3} \quad (i=4-6) \tag{9}$$

for the components related with the rigid body modes, and by

$$\partial\Phi_i/\partial n=i\omega u_{in} \quad \left(i>6\right) \tag{10}$$

for the components related with the elastic modes. Here, $i\omega$ is from the harmonic time dependence, **n** is the unit normal vector on $S_w$ pointing out of the fluid domain, **r** is the position vector, and $u_{in}$ denotes the displacement of the structure along **n** for the elastic modes, with the first one corresponding to $i$ = 7, second to $i$ = 8, and so on. For the diffraction potential $\Phi_D$, the body is taken in a fixed position so that the kinematic boundary condition on $S_w$ becomes

$$\partial\Phi_D/\partial n = \partial\left(\Phi_I + \Phi_S\right)/\partial n = 0 \quad \text{on } S_w \tag{11}$$

$\Phi_i$ and $\Phi_S$ satisfy also the free surface boundary condition on $S_f$:

$$\partial\left(\Phi_I, \Phi_S\right)/\partial z = \left(\omega^2 / g\right)\left(\Phi_I, \Phi_S\right) \quad \text{on } S_f \tag{12}$$

The fluid perturbations except the incident waves radiate away from the body. For the infinite fluid domain, the additional radiation condition states that the effects of the body on fluid domain will diminish and ensures a unique solution of the problem [11]. Since water is taken deep, no bottom condition is imposed here.

### 2.3. Boundary element solution of the potential problem

The boundary value problem for the radiation and diffraction potentials, defined by the Laplace equation and boundary conditions (8)-(12), can be expressed by a BIE over the wetted surface of the structure, by adopting the wave Green function as the fundamental solution:

$$c(\boldsymbol{\xi})\Phi(\boldsymbol{\xi}) + \int_{S_w} \Phi(\mathbf{x}) G_{,n}(\mathbf{x},\boldsymbol{\xi}) da = \int_{S_w} \Phi_{,n}(\mathbf{x}) G(\mathbf{x},\boldsymbol{\xi}) da \tag{13}$$

Here, $\Phi$ represents $\Phi_R$ and $\Phi_D$, $G(\mathbf{x}, \boldsymbol{\xi})$ is the free surface Green function, $\boldsymbol{\xi} = (\xi, \eta, \zeta)^T$ and **x** denote the source and field points of the Green function on $S_w$, respectively, and $(\,)_{,n} = \partial(\,)/\partial n$ indicates flux. The free term $c(\boldsymbol{\xi})$ is due to the singular nature of $G_{,n}$; it identifies the fraction of $\Phi(\boldsymbol{\xi})$ that lies inside the fluid domain. For a three-dimensional homogenous field, the Green function can be given by

$$4\pi G = \frac{1}{r} + \frac{1}{r'} + 2f N_0(h,v) + 2\pi f\left(E_0(h) + iJ_0(h)\right)e^v \tag{14}$$

Here, $r$ is the distance between the field and source points, $r'$ is the distance between the field point and free-surface image of the source point, $f = \omega^2 L/g$ is the non-dimensional frequency parameter with $L$ characterizing the length of the radiating and diffracting body, $h$ and $v$ represent the horizontal components of $r$ and vertical component of $r'$, respectively, $J_0$ is the Bessel function of the first kind and zeroth order, and $E_0$ is the Weber function. In Eq. (14), $N_0$ represents the non-oscillatory local flow disturbance and the last term represents the circular surface waves radiating away from the source point $\boldsymbol{\xi}$ [12]. Since Eq. (14) satisfies the free surface boundary condition and radiation condition implicitly, Eq. (13) is defined over $S_w$, instead of the total fluid boundary surface, comprising $S_w$, $S_f$, and $S_\infty$, the control surface considered at infinity.

For the numerical solution of Eq. (13), $S_w$ is discretized as a collection of surface boundary elements, over which the potential function and flux distributions are approximated using the shape functions and related nodal values. For the $i$th boundary element, the corresponding representations, $\Phi^j$ and $\Phi^i_{,n}$, are given as

$$\Phi^i = \sum_{j=1}^{n_i} \Phi_{ij} N_j(s,t) \;,\; \Phi^i_{,n} = \sum_{j=1}^{n_i} (\Phi_{,n})_{ij} N_j(s,t), \tag{15}$$

where $n_i$ is the number of nodal points assigned to the element, $\Phi_{ij}$ and $(\Phi_{,n})_{ij}$ respectively represent the potential and flux values at $j$th node of the element, and $N_j$ denotes the associated shape function, with $s$, $t$ indicating the local coordinates.

By consecutively taking the nodal points of the discretization as the source point for Eq. (13) and using the definitions (15), the potential distributions over the wetted surface of the floating structure can be expressed by the following set of algebraic equations:

$$c_k \Phi_k + \sum_{i=1}^{n_e} \sum_{j=1}^{n_i} \Phi_{ij} \int_{S_i} N_j G_{,n} da = \sum_{i=1}^{n_e} \sum_{j=1}^{n_i} (\Phi_{,n})_{ij} \int_{S_i} N_j G \, da \qquad k = 1,...,n_n \tag{16}$$

Here, $n_n$ and $n_e$ are the total numbers of nodes and boundary elements used in the discretization, respectively, $S_i$ is the area of the $i$th boundary element, and $\Phi_k$ denotes the potential of the $k$th nodal point. After completing the surface integrations and considering the radiation potential components by applying appropriate kinematical boundary condition for $\Phi_{,n}$, depending on the associated mode shape, the resulting system of equations for the radiation potential can be given as

$$\mathbf{H}(\omega)\left(\mathbf{\Phi}_1 ..... \mathbf{\Phi}_{n_m}\right) = i\omega \mathbf{G}(\omega)\left(\mathbf{w}_1 ..... \mathbf{w}_{n_m}\right) \tag{17}$$

$\mathbf{\Phi}_i$ is the vector of nodal potentials here and $\mathbf{w}_i$ represents the right hand sides in Eqs. (8)-(10), i.e., stands for $\mathbf{u}_{in}$ for elastic modes. $\mathbf{G}$ and $\mathbf{H}$ represent the frequency dependent, complex valued surface integrals involving the wave Green function and its flux; their components represent the boundary element interactions between nodes. The resulting $\mathbf{\Phi}_i$ distributions can be obtained from the solution of Eq. (17).

A similar solution course can be followed for the diffraction potential by enforcing the condition $\Phi_{S,n} = -\Phi_{I,n}$ on $S_w$ from Eq. (11). By applying the Haskind relations [11], however, the diffraction problem is avoided in this study and the related wave excitation forces are directly calculated by using the radiation potential solution.

### 2.4. The extended boundary integral equation formulation

When the wave Green function is used as the fundamental solution of the boundary integral equation (13), as in this study, the solution becomes non-unique at certain frequencies, which correspond to the eigenfrequencies of the non-physical Dirichlet-type problem of internal fluid sloshing. For eliminating the irregular frequencies, an extended boundary integral equation method [9] is adopted in this study. The fundamental idea of the method is extending the computational domain by the assumed internal free surface, over which the fluid motion is suppressed, i.e., covered with a rigid lid. Accordingly, Eq. (17) can be rewritten for the radiation potential component $\mathbf{\Phi}_i$ as

$$\begin{bmatrix} \mathbf{H}^{bb} & \mathbf{H}^{bf} \\ \mathbf{H}^{fb} & \mathbf{H}^{ff} \end{bmatrix} \begin{pmatrix} \mathbf{\Phi}_i^b \\ \mathbf{\Phi}_i^f \end{pmatrix} = i\omega \begin{bmatrix} \mathbf{G}^{bb} & \mathbf{G}^{bf} \\ \mathbf{G}^{fb} & \mathbf{G}^{ff} \end{bmatrix} \begin{pmatrix} \mathbf{w}_i^b \\ \mathbf{w}_i^f \end{pmatrix} \tag{18}$$

Here, $\mathbf{H}$ and $\mathbf{G}$ matrices as well as $\mathbf{\Phi}$ and $\mathbf{w}$ vectors are decomposed into body and internal free surface related parts, where superscripts $b$ and $f$ refer to the body and free surface associations, respectively; e.g., $\mathbf{\Phi}^b$ contains the potential values over $S_w$, whereas $\mathbf{H}^{bf}$ is constructed by taking the source points as the body nodes and field points as the free surface nodes in boundary element expressions. The unmodified system composed of the matrices with the $bb$ attachment, so that the computational load seems to rise significantly. However, since they are related with the rigid wall condition imposed over the free surface, the sub matrices $\mathbf{G}^{ff}$ and $\mathbf{G}^{bf}$ are avoided in practice, and the number of free surface nodes are expected to be smaller than the number of wetted surface nodes, which together result a limited overload, in general. The

solution of Eq. (18) for $\mathbf{\Phi}_i$ will return the potential distribution over $S_w$ free from the irregular frequency effects.

### 2.5. Generalized hydrodynamic forces

By neglecting the second-order terms and hydrostatic component in the Bernoulli's equation, the dynamic fluid pressure, $P$, can be given as $P = -\rho_f \Phi_{,t}$. Using the potential decomposition, we can write

$$P = -i\omega\rho_f \left( \zeta \left( \Phi_I + \Phi_S \right) + \sum_{i=1}^{n_m} \Phi_i p_i \right) e^{i\omega t}, \tag{19}$$

where $\rho_f$ is the fluid density, $\zeta$ is the incident wave amplitude, and multiplication by $i\omega$ is due to the harmonic time dependence. The hydrodynamic force acting on the structure is defined by integrating the fluid pressure (19) over $S_w$ and its amplitude is given by

$$\mathbf{f} = -i\omega\zeta\rho_f \int_{S_w} \mathbf{n} \left( \Phi_I + \Phi_S \right) da - i\omega\rho_f \sum_{i=1}^{n_m} p_i \int_{S_w} \mathbf{n} \Phi_i \, da \tag{20}$$

The first term is due to the diffraction problem and represents the wave excitation forces, in proportion to the wave amplitude; the second term is related with the radiation problem and it defines the radiation force, also known as the fluid-structure interaction force since it results from the interaction through the kinematic boundary condition.

Using the definition of generalized force, given in Section 2.1, and substituting the radiation potential distribution obtained from Eq. (17) into Eq. (20), the generalized radiation force can be expressed as

$$\tilde{\mathbf{f}}(\omega) = \left( \omega^2 \mathbf{A}(\omega) - i\omega \mathbf{B}(\omega) \right) \mathbf{p}, \tag{21}$$

where **A** and **B** are the generalized matrices of added-mass and hydrodynamic damping, respectively, with the components

$$A_{ij} = \rho_f \int_{S_w} \mathbf{w}_i \, \mathrm{Re}\left( \mathbf{H}^{-1}\mathbf{G} \right) \mathbf{w}_j \, da \,, \; B_{ij} = -\rho_f \omega \int_{S_w} \mathbf{w}_i \, \mathrm{Im}\left( \mathbf{H}^{-1}\mathbf{G} \right) \mathbf{w}_j \, da \tag{22}$$

By using the Haskind relations, the generalized wave excitation force, $\mathbf{f}_w$, can be directly obtained in terms of incident and radiation potential distributions without using the scattering potential field. The $i$th component can be written as

$$\tilde{f}_{wi} = -\rho_f \int_{S_w} \left( \Phi_I \Phi_{i,n} - \Phi_{I,n} \Phi_i \right) da \tag{23}$$

and using Eq. (17) becomes

$$\tilde{f}_{wi} = -i\omega\rho_f \int_{S_w} \left( \mathbf{\Phi}_I - \mathbf{\Phi}_{I,n} \mathbf{H}^{-1}\mathbf{G} \right) \mathbf{w}_i \, da \tag{24}$$

By substituting the generalized wave radiation and excitation forces from Eqs. (21), and (24), the generalized equation of motion, Eq. (4), of the floating structure that is subjected to regular waves becomes

$$\left( -\omega^2 \left( \tilde{\mathbf{M}} + \mathbf{A}(\omega) \right) + i\omega \mathbf{B}(\omega) + \tilde{\mathbf{K}} \right) \mathbf{p} = \tilde{\mathbf{f}}_w(\omega) \tag{25}$$

Here, the structural damping and the restoring force due to hydrostatic pressure is neglected. The dynamic response of the structure can be obtained by using the principal coordinate vector obtained from the solution of Eq. (25) in the modal expansion (3), for each wave frequency.

## 3. NUMERICAL APPLICATIONS

To study the performance of the EBIEM for eliminating the irregular frequencies that are inherent to the BEM solution of wave-structure interaction problems and also investigate the effect of participating factors within the process, two free-floating surface piercing structures are selected for application: a cylinder, which is essentially used to verify the analysis method, and a large floating plate that significantly challenges the suppression procedure, especially at high frequencies. The discussion mainly encloses the effect of discretization regarding the wetted body and internal free surfaces, in terms of mesh fineness and element order, on regularizing the hydrodynamic forces. For the purpose of comparison and assessment, the radiation and wave excitation forces associated with the rigid body modes (for the cylinder) and elastic modes (for the plate) are used. The higher-order BEM implementation is conducted through four-noded linear and eight-noded quadratic isoparametric elements. The wetted surface is discretized using only linear elements; the internal surface is discretized using both linear and quadratic elements. Adopted idealizations, referred to as models, are identified by the number of elements distributed over the wetted surface and internal free surface, which are identified as NE and NEF, respectively.

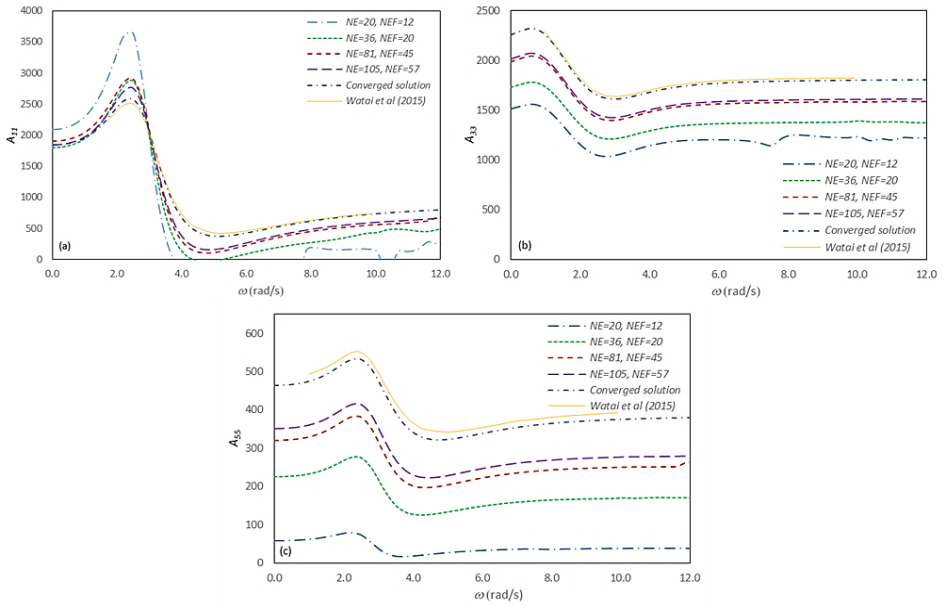


**Figure 1.** Generalized added mass coefficients of the cylinder due to the motions (a) surge, (b) heave, (c) pitch

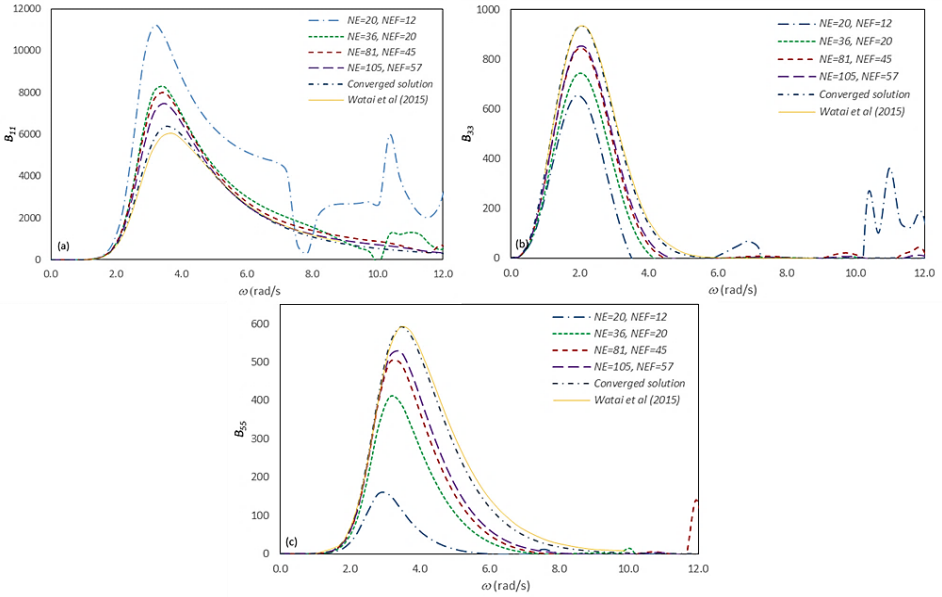


**Figure 2.** Generalized hydrodynamic damping coefficients of the cylinder due to the motions (a) surge, (b) heave, (c) pitch

The studied floating cylinder has 1 m radius and 1 m draught and the fluid density is taken as 1000 kg/m$^3$. Four relatively coarser models are used to display the convergence of the results and also to demonstrate the efficiency of the EBIEM when only a few irregular frequencies are observed with weak disruptive effects, at least for some of the principal indicators. These models, identified as (NE, NEF), are (20, 12), (36, 20), (81, 45), and (105, 57). A fine model comprising dense meshes are additionally adopted to present the converged BEM results.

The predictions for the diagonal components of the generalized added mass and hydrodynamic damping matrices that are associated with the surge, heave and pitch motions of the cylinder are presented in Figs. 1 and 2, respectively, and compared with the numerical results of [13]. The smooth convergence attained with better models and close agreement between the converged results and reference values are apparent for all force components, even though the pitch related components converge slower than others. Focusing on the irregular frequencies, the effects are more noticeable for surge and heave motions and also for hydrodynamic damping coefficients. The first model clearly suffers from the effects after $\omega = 6$ rad/s. By slightly refining the model, the effects are quite reduced and the first observed irregular frequency is postponed to after $\omega = 9$ rad/s. After two similar refinements, the irregular frequencies are completely eliminated all along the studied frequency interval. They persist to exist, however, for higher frequencies (not shown here), and keep polluting the results within contained regions. The generalized wave excitation forces due to surge, heave and pitch motions of the cylinder, given in Fig. 3, exhibits the same behavior, but more explicitly. Similar to the radiation forces, finer models lead to better performance of the EBIEM for reducing the irregular frequency effects, but even the fourth model is far from a sufficient regularization. The converged solution, however, fairly agrees with the results of [13] and only a slight trace of irregularity exists at high frequencies.

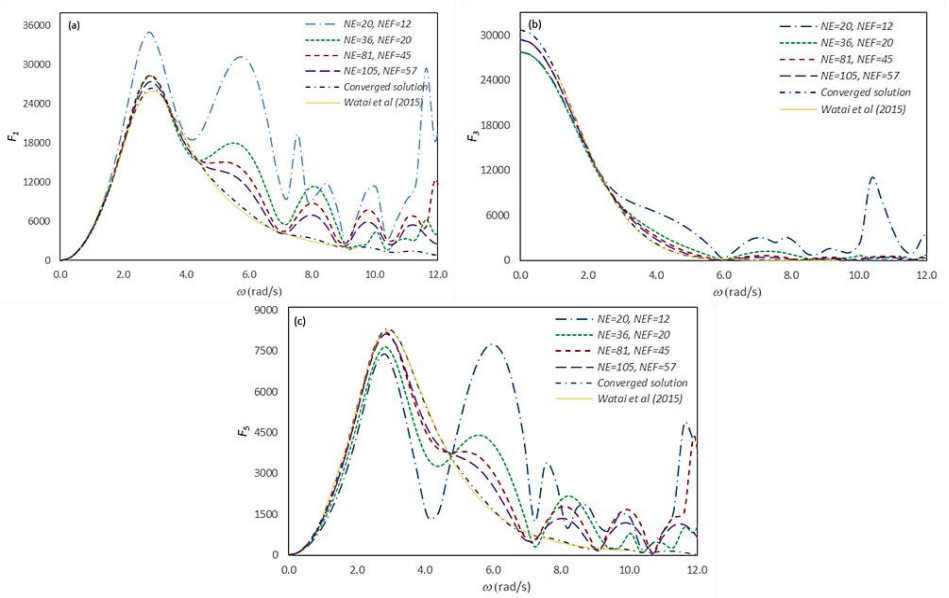


**Figure 3.** Generalized wave excitation forces of the cylinder due to the motions
(a) surge, (b) heave, (c) pitch

The second set of computations is related with the elastic motions of a large floating plate. With its very small thickness, hence draught, the influence of the free surface effects on dynamic behavior will be large, so that the presence of irregular frequencies and their effects on results are expected to be strong, leading to a more compelling test for the EBIEM. The geometric and material properties of the plate are given in Table 1. The surrounding fluid is fresh water of 1025 kg/m$^3$ density. The wave radiation and excitation forces due to the first six modes of the plate are presented; corresponding mode shapes, each associated with vertical bending (VB), horizontal bending (HB), or torsion (T), can be seen in Fig. 4. Three different discretization of wetted surface and internal free surface are used for the analysis with NE values of 756, 1168, 1660, and 2232, and NEF values of 360, 640, and 1000. Unlike the cylinder problem, where the linear free surface elements provide sufficient suppression at the end, both linear and quadratic free surface elements are adopted in this case. The diagonal components of the generalized added mass and hydrodynamic damping forces, and the components of the generalized wave excitation force are presented.

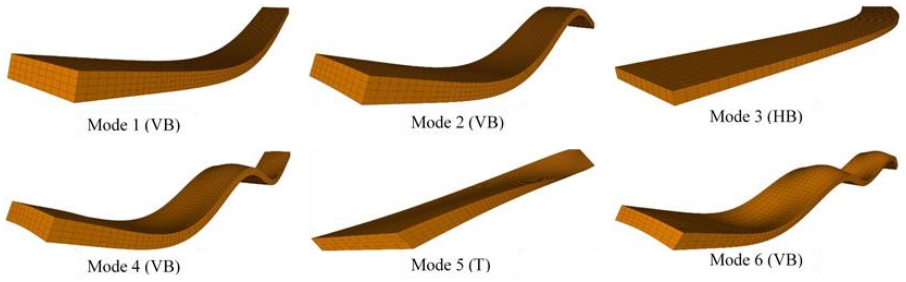


**Figure 4.** First six elastic mode shapes of the floating plate

**Table 1.** Geometric and structural properties of the floating plate

| | |
|---|---|
| Length | 100 m |
| Breadth | 10 m |
| Height | 2 m |
| Draught | 1 m |
| Mass | 1025 ton |
| Elastic Modulus | 15 GPa |
| Poisson's Ratio | 0.3 |

In Fig. 5, the generalized added mass coefficients that are obtained using the model (756, 640) and by adopting both linear (L) and quadratic (Q) free surface elements are given for the first, second, and fourth modes. Up to $\omega$ = 4 rad/s, two group of results nicely agree, after which the irregular frequencies appear, ruining all predictions. Quadratic results, however, are less affected, giving a hint of being a better option to deal with the pollution.

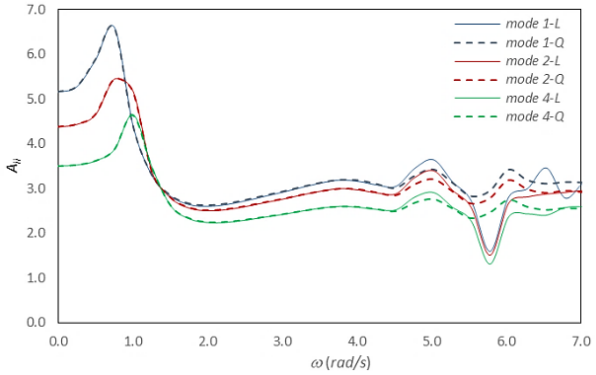


**Figure 5.** Generalized added mass coefficients of the plate obtained using the model (756, 640)

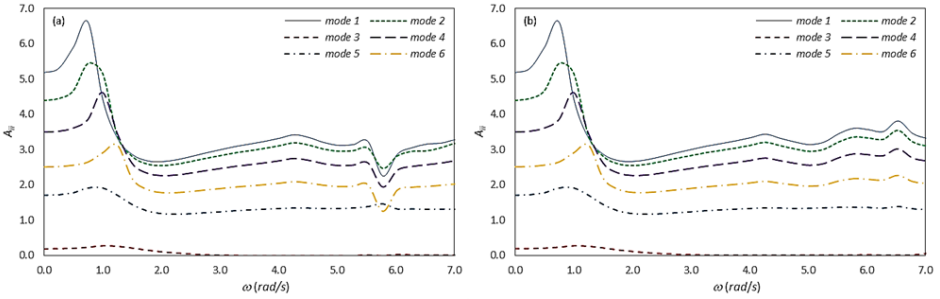


**Figure 6.** Generalized added mass coefficients due to the first six modes of the plate obtained using linear free surface elements and (a) model (1186, 640), (b) model (1186, 1000)

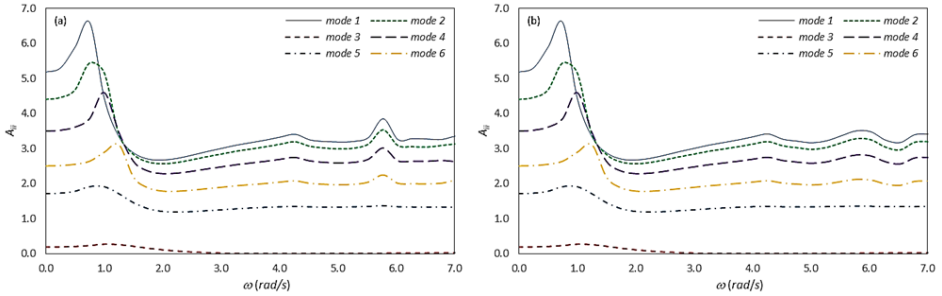


**Figure 7.** Generalized added mass coefficients due to the first six modes of the plate obtained using quadratic free surface elements and (a) model (1186, 640), (b) model (1186, 1000)

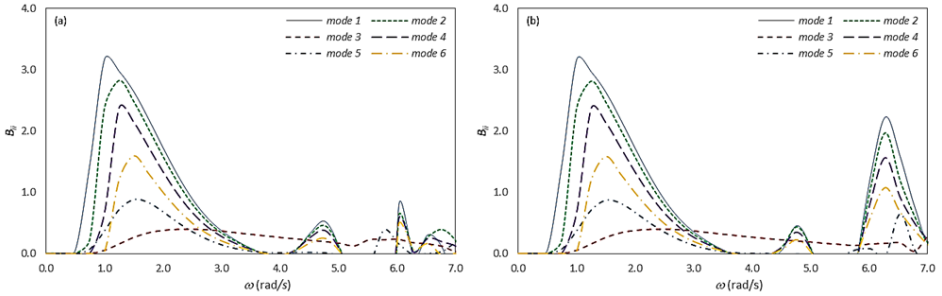


**Figure 8.** Generalized hydrodynamic damping coefficients due to the first six modes of the plate obtained using linear free surface elements and (a) model (1186, 640), (b) model (1186, 1000)

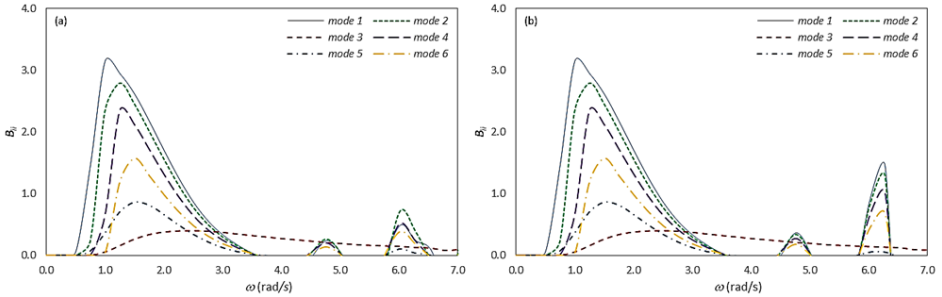


**Figure 9.** Generalized hydrodynamic damping coefficients due to the first six modes of the plate obtained using quadratic free surface elements and (a) model (1186, 640), (b) model (1186, 1000)

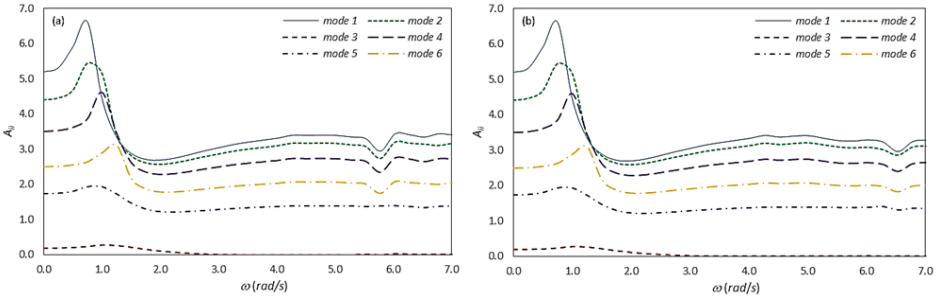


**Figure 10.** Generalized added mass coefficients due to the first six modes of the plate obtained using linear free surface elements and (a) model (1660, 640), (b) model (1660, 1000)

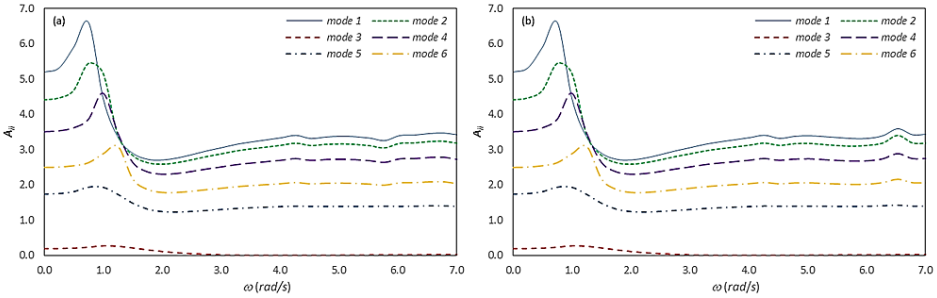


**Figure 11.** Generalized added mass coefficients due to the first six modes of the plate obtained using quadratic free surface elements and (a) model (1660, 640), (b) model (1660, 1000)

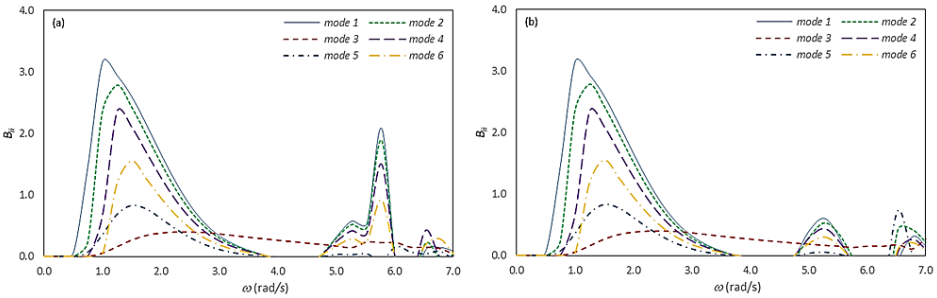


**Figure 12.** Generalized hydrodynamic damping coefficients due to the first six modes of the plate obtained using linear free surface elements and (a) model (1660, 640), (b) model (1660, 1000)

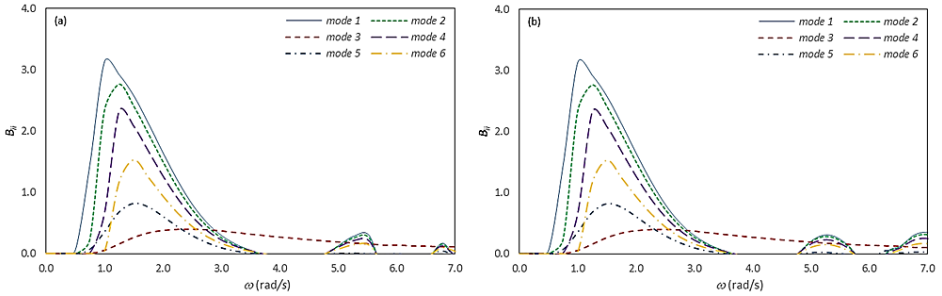


**Figure 13.** Generalized hydrodynamic damping coefficients due to the first six modes of the plate obtained using quadratic free surface elements and (a) model (1660, 640), (b) model (1660, 1000)

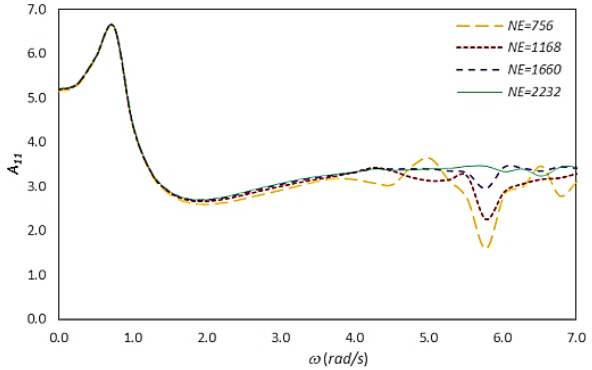


**Figure 14.** $A_{11}$ value obtained using NEF = 640 and four different NE values

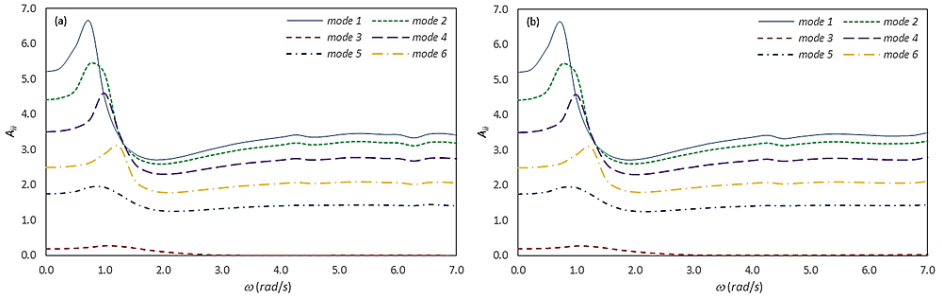


**Figure 15.** Generalized added mass coefficients due to the first six modes of the plate obtained using the model (2232, 1000) and (a) linear free surface elements, (b) quadratic free surface elements

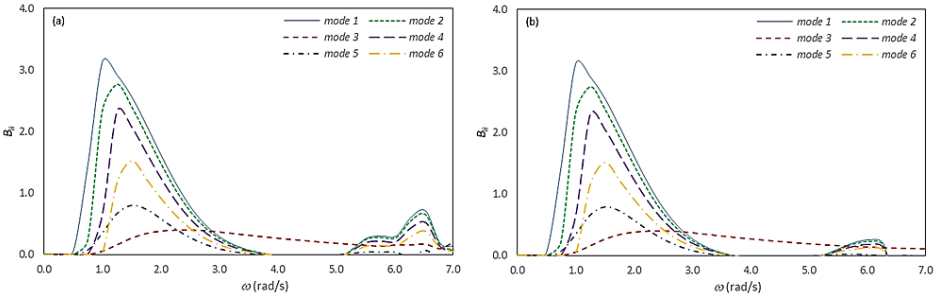


**Figure 16.** Generalized hydrodynamic damping coefficients due to the first six modes of the plate obtained using the model (2232, 1000) and (a) linear free surface elements, (b) quadratic free surface elements

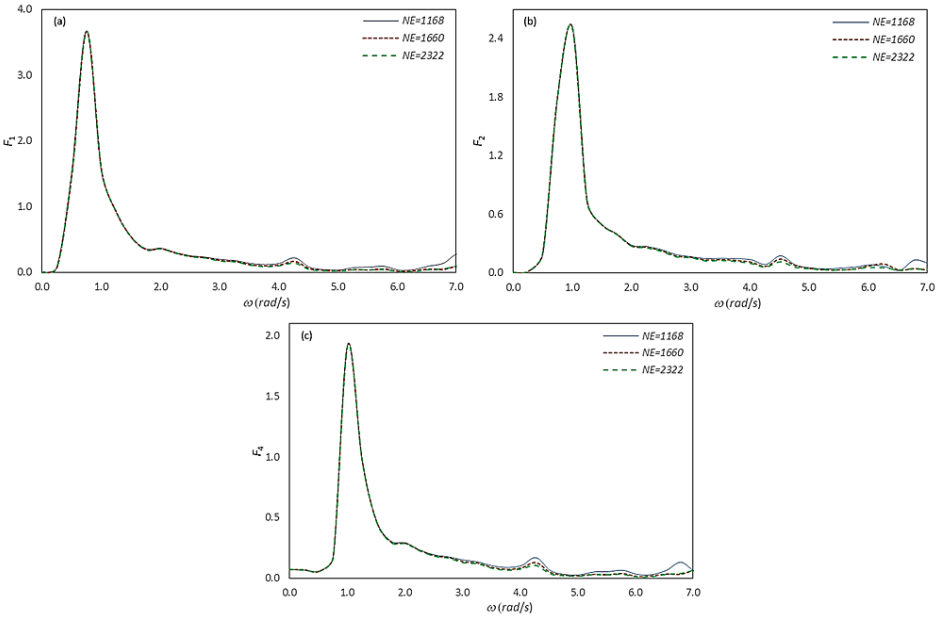


**Figure 17.** The generalized wave excitation force components of the plate obtained using linear free surface elements with NEF = 1000 and NE = 1168, 1660, 2322, and due to the (a) first mode, (b) second mode, (c) fourth mode

The added mass and hydrodynamic damping coefficients due to the first six modes are presented in Figs. 6-9, where the models (1186, 640) and (1186, 1000) with linear (Figs. 6, 8) and quadratic (Figs. 7, 9) free surface elements are adopted. The irregularities in added mass coefficients are visibly reduced compared to the previous case, but unlike the cylinder problem, the irregular frequencies are not postponed either with increasing the NE or NEF value. In addition, the difference between the linear and quadratic elements are less apparent. As for the cylinder problem, the influence of irregular frequencies on damping coefficients is more severe. The results of another mesh refinement is given in Figs. 10-13. NE value is increased to 1660 this time, but NE values are still 640 and 1000. It is becoming clear that increasing the NE value for a

fixed value of NEF is more effective than increasing the NEF value for a fixed value of NE. It should be pointed that, however, this is not related with the 'convergence of results.' As can be seen from Fig. 14, where $A_{11}$ value obtained using four different NE values for the same NEF value is presented, that the predictions of coarsest and finest wetted surface meshes are almost same within the regular region; the mesh quality starts to pay off when the irregular frequencies are being observed. The results of final refinement are given in Figs. 15, 16, where the model (2232, 1000) is adopted. Now, the irregular frequencies are almost suppressed, yet traces can be observed, especially for the damping coefficients.

The first, second, and fourth components of the generalized wave excitation force for the floating plate are given in Figs. 17 and 18, considering linear and quadratic free surface elements, respectively, for NE values of 1168, 1660, 2322, and NEF value of 1000. The finer two models are almost identical and some irregular frequency effects can be observed even with quadratic elements. This is not surprising, since the wave excitation are obtained using the Haskind relations, which rely on the radiation forces that possess irregularities.

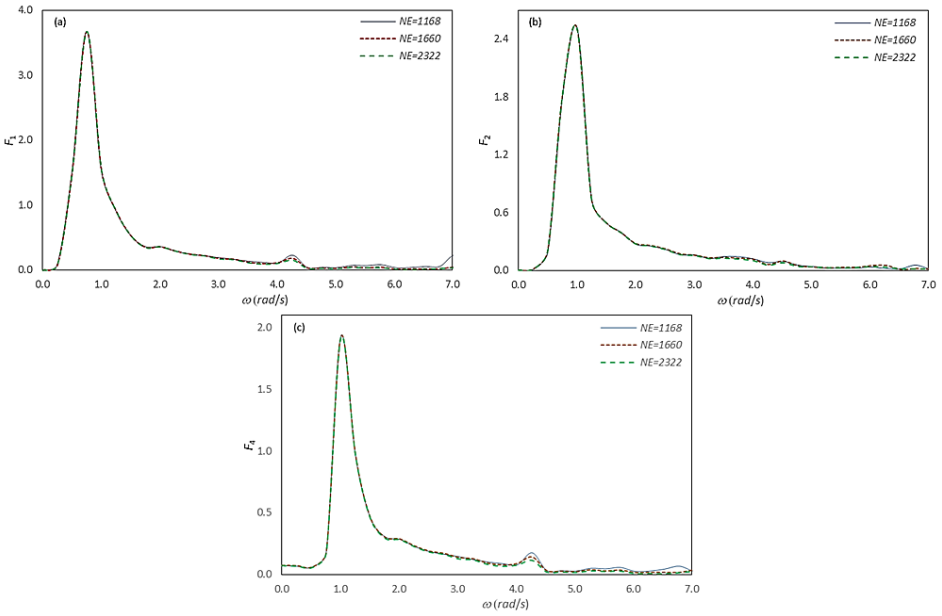


**Figure 18.** The generalized wave excitation force components of the plate obtained using quadratic free surface elements with NEF = 1000 and NE = 1168, 1660, 2322, and due to the (a) first mode, (b) second mode, (c) fourth mode

## 4. CONCLUSIONS

Performance of the extended boundary integral equation method (EBIEM) for eliminating the irregular frequencies that are inherent to the wave Green function based boundary element solution of the frequency domain wave-body interaction problems is investigated. The EBIEM is based on the idea that the non-physical internal fluid motion that is associated with the irregular frequencies can be suppressed by including the assumed internal free surface into the computational domain and covering it by a rigid lid, i.e., applying the rigid wall boundary condition over it. Two surface piercing structures, a cylinder and a large plate, are selected for

application; the focus is on the influence of internal free surface discretization, depending on the mesh fineness and element order, for the regularization of the radiation and wave excitation forces, where both rigid body and elastic modes are considered. Some conclusions are given as follows:

- The method provides excellent predictions for the radiation forces due to the rigid body modes of the free floating cylinder. The irregular frequency effects, existing in relatively mild form, are effectively eliminated within the studied frequency interval, but it is observed that they persist to exist for higher frequencies. This suggest that even though the EBIEM is proposed as a complete removal technique, it is rather postponing the occurrence of irregular frequencies.
- The second case of floating plate, the real testbed for studying the limits of the procedure, clearly indicates that the mesh refinement is essential for successful application of the EBIEM. Refining either the wetted surface or internal free surface weakens the irregular frequency effects, but effect of the former is more evident. It should be pointed that this is not related with the convergence of the numerical model, contrary a feature that is seen at the already converged results.
- The benefit of using better representations are twofold, in general: deferring the first observed frequency and reducing both the effects and extent of the influenced zone.
- Quadratic elements perform better than linear elements, especially when the wetted surface mesh is relatively coarse. Nevertheless, considering the increase of the degrees of freedom, hence computation time, for the same number of elements, the benefit is questionable for finer models, where the performance gap between linear and quadratic elements is narrow.
- The effects are consistently much more visible for the hydrodynamic damping coefficients compared to the added mass coefficients; this is unexpected, since they are related with the same radiation force. This may also have a negative side effect on the wave excitation forces, because the adopted Haskind relations rely on the use of radiation forces for their computation. Both added mass and hydrodynamic damping coefficients are frequency dependent and they are related with the same time dependent impulse response functions through the Fourier transform, but in different forms. It may be an interesting exercise to obtain the time domain counterparts using the added mass values and then to compute the hydrodynamic damping values by applying the inverse transform to the impulse response functions.

## REFERENCES

[1] John, F., (1950) On the motion of floating bodies II. Simple harmonic motions, *Communications on Pure and Applied Mathematics* 3, 45-101.

[2] Burton, A.J., Miller, G.F., (1971) The application of integral equation methods to the numerical solution of some exterior boundary-value problems, *Proceedings of the Royal Society of London. A. Mathematical and Physical Sciences* 323, 201-210.

[3] Schenck, H.A., (1968) Improved integral formulation for acoustic radiation problems, *The Journal of the Acoustical Society of America* 44, 41-58.

[4] Kleinman, R.E., (1982) On the mathematical theory of the motion of floating bodies - an update, *Technical report*, No: 82/074, David Taylor Naval Ship Research and Development Center.

[5] Lee, C.H., Sclavounos, P.D, (1996) Removing the irregular frequencies from integral equations in wave-body interactions, *Journal of Fluid Mechanics* 207, 393-418.

[6] Lau, S.M., Hearn, G.E., (1989) Suppression of irregular frequency effects in fluid–structure interaction problems using a combined boundary integral equation method, *International Journal for Numerical Methods in Fluids* 9, 763-782.

[7] Liapis, S., (1993) A method for suppressing the irregular frequencies from integral equations in water wave-structure Interaction problems, *Computational Mechanics* 12, 59-68.

[8] Ohmatsu, S., (1975) On the irregular frequencies in the theory of oscillating bodies in a free surface, *Papers of Ship Research Institute Tokyo* 48, 1-13.

[9] Lee, C.H., Newman, J.N., Zhu, X., (1996) An extended boundary integral equation method for the removal of irregular frequency effects, *International Journal for Numerical Methods in Fluids* 23, 637-660.

[10] Liu, Y., Falzarano, J.M., (2017) A method to remove irregular frequencies and log singularity evaluation in wave-body interaction problems, *Journal of Ocean Engineering and Marine Energy* 3, 161-189.

[11] Newman, J.N., (1977) Marine Hydrodynamics. *MIT Press*, Cambridge.

[12] Telste, J.G., Noblesse, F., (1986) Numerical Evaluation of the Green-Function of Water-Wave Radiation and Diffraction, *Journal of Ship Research* 30, 69-84.

[13] Watai, R.A., Ruggeri, F., Sampaio, C.M.P., Simos, A.N., (2015) Development of a time domain boundary element method for numerical analysis of floating bodies' responses in waves, *Journal of the Brazilian Society of Mechanical Sciences and Engineering* 37, 1569-1589.